Analysis and design tool for optical multipass systems modeled with parametric surfaces

Olga M. Conde*, Adolfo Cobo, Francisco J. Madruga, M. Ángeles Quintela, José M. López-Higuera
Grupo de Ingeniería Fotónica; Dept. T.E.I.S.A.
Universidad de Cantabria, Avda.Los Castros s/n, 39005 Santander, Spain

ABSTRACT

A novel software tool has been developed to improve and optimize the design of optical multipass cells in long-path absorption spectroscopy. One of the main application fields of these cells is the monitoring of hazardous gases, where they become the transducers of a global fiber optic sensor. New techniques, based on solids modeling, have been applied for the description of the mirrors that constitute the multipass cell. These mirrors have been represented in terms of parametric surfaces known as NURBS (Non-Uniform Rational B-Spline). Under this approach, the design can reach a high degree of flexibility and versatility. The behavior of the multipass cell has been evaluated by means of different specific ray-tracing techniques that have been implemented taking into account the parametric nature of NURBS surfaces.

Keywords: Optical multipass cells, parametric surfaces, ray-tracing methods, optical resonators.

1. INTRODUCTION

The detection of dangerous gases through optical methods depends directly on the ability to manufacture gas cells able to keep the compound to be detected in contact with the optical source employed for the monitorization. This operation requires that gas and light will be in contact as much time as possible. The more this requirement is accomplished; the most sensitive would be the measurement of the gas. This fact is directly related with the time that the light beam is maintained within the cell, becoming fundamental that the length of the optical path followed inside the cell becomes maximum. Initial works in the design of optical resonators are attributable to White [1] and Herriot [2]. Both of them utilize canonical structures as spherical o parabolic surfaces to model the mirrors. With these structures, the pattern formed by the reflection points follows an elliptical projection and different number of reflections can be attained by separating the mirrors but, at the end, this is limited by the structure itself. To overcome this problem and to gain in efficiency in path length with respect to the cell volume, as well as to reduce interference effects between reflection points, cells with astigmatic mirrors can be employed [3]. The main handicap arising with these mirrors is that their design is not so obvious.

With the aim of helping in the design of astigmatic multipass cells, a new tool is presented in this contribution. This tool is able to perform the analysis of a specific multipass cell by means of ray-tracing techniques. The main advantage of this new tool is its ability to cope with surfaces whose shape can be completely arbitrary avoiding the restrictions of the canonical ones. In the novel tool, the mirrors are modeled by parametric surfaces of arbitrary order that allow to represent from canonical structures, such as spherical or parabolic, to the more complicated ones just by changing the surface parameters. The selected parametric surface has been taken from the automotive and aeronautic design field favoring the manufacturing of the final designed mirror. CAD/CAM equipment can be found in the market that directly accepts this surface format and no translations are needed into simple structures avoiding the well-known translation errors. Two different ray-tracing mechanisms have been implemented and compared for different case analysis. Results have been also compared with published work.

Section 2 describes briefly the geometrical representation adopted for the mirrors of the multipass cell and how the optical source has been modeled. Section 3 makes emphasis in the two ray-tracing algorithms implemented. Section 4 will show the results attained with the present tool and, finally, section 5 outlines the conclusions extracted from this work.

* olga.conde@unican.es; Tel: + 34 942 201539; Fax: + 34 942 200877; http://grupos.unican.es/gif

Optical Design and Engineering, edited by Laurent Mazuray,
Philip J. Rogers, Rolf Wartmann, Proceedings of SPIE Vol. 5249
(SPIE, Bellingham, WA, 2004) · 0277-786X/04/$15 · doi: 10.1117/12.513291

2. CELL DESCRIPTION

The typical configuration of an optical multipass cell or an optical resonator includes a closed volume with mirrors at its extremes where the light beam bounces back and forth achieving the desired long path confinement. Several approaches could be followed to model the mirrors surfaces: sets of flat polygons but this arises geometrical inaccuracies, canonical surfaces that would reduce the scope of the application, etc. In this work, the selected approach is the use of completely arbitrary parametric surfaces called NURBS (*Non-Uniform Rational B-Spline*) [4] widely known in the *Computer Aided Geometric Design* field (*CAGD*) and initially created for the automotive and aeronautic design environment. Due to its importance in the solid modeling world, these surfaces have become standard entities of geometric design languages such as IGES (*Initial Graphics Exchange Specification*) so it will be easy to find CAD/CAM equipment able to translate, into the manufacturing process, the design proposed by the analysis and design tool. The main advantage of this kind of parametric surfaces resides on its ability to represent, in an accurate way, different types of surfaces applying the same notational structure.

In this work, another refinement has been done. As the NURBS representation becomes numerically unstable when certain geometrical vectors have to be calculated on points of the surface, a conversion to Bézier surfaces has been implemented following the Cox-de-Boor algorithm [5]. Basically, a Bézier surface is also a parametric surface defined by the expression (1):

$$\bar{r}(u,v) = \frac{\bar{N}(u,v)}{D(u,v)} = \frac{\sum_{i=0}^{m}\sum_{j=0}^{n} \bar{p}_{ij} \cdot w_{ij} \cdot B_i^m(u) \cdot B_j^n(v)}{\sum_{i=0}^{m}\sum_{j=0}^{n} w_{ij} \cdot B_i^m(u) \cdot B_j^n(v)} \tag{1}$$

where (u,v) are the parametric coordinates of an specific point on the surface; $\bar{p}_{ij}$ are the control points of the surface given in Cartesian coordinates (x,y,z), these points constitute the control network that geometrically represents the convex envelope of the Bézier surface; w_{ij} are the weights of the control points, i.e. how the surface approaches the control points $\bar{p}_{ij}$; $B_i^m(u)$ is the Bernstein basis for a parametric coordinate u and degree m that is defined in expression (2); finally m and n are the degrees of the Bernstein basis in each parametric direction used by the lineal combination that defines the surface.

$$B_i^n(t) = \binom{n}{i} t^i (1-t)^{n-i} \qquad where \qquad \binom{n}{i} = \begin{cases} \dfrac{n!}{i!(n-i)!} & if\ 0 \le i \le n \\ 0 & elsewhere \end{cases} \tag{2}$$

To provide a graphical insight of a Bézier surface, figure 1 shows the main associated parameters. Changes from one surface to another are achieved just by modifying the degrees m and n or the position and weights of the control points. These surfaces range from the canonical ones, such as flat plates, spheres, parabolic, etc., to completely arbitrary ones.

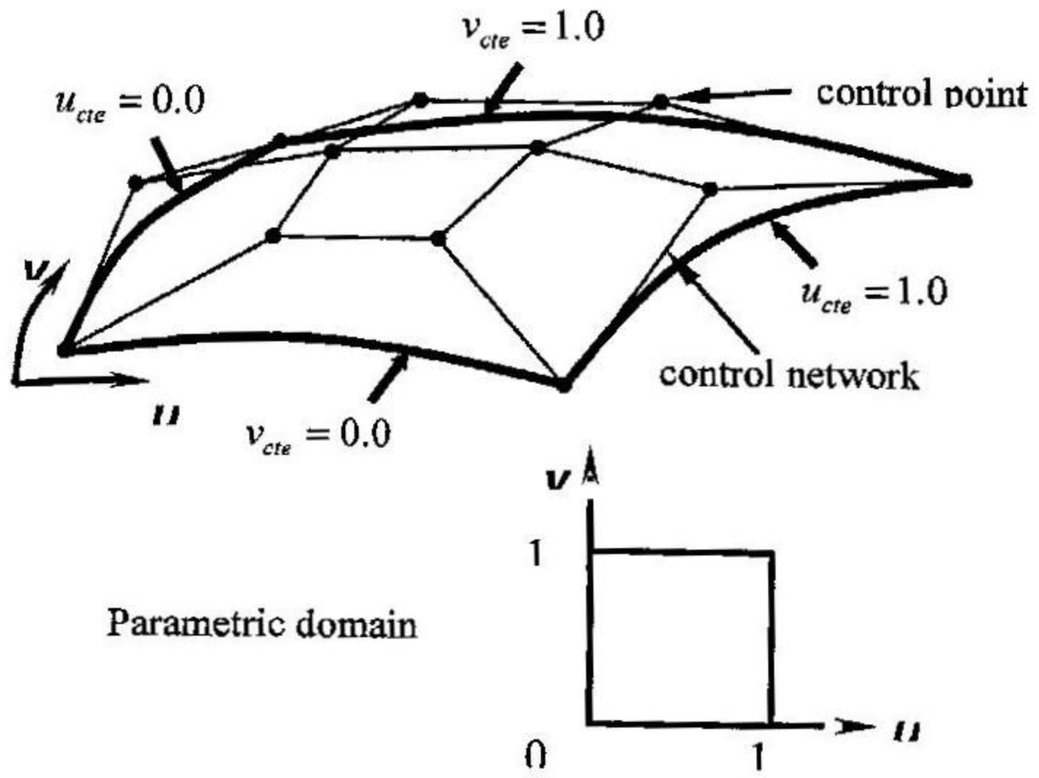

Figure 1: Definition of a Bézier surface: control points and network.

But this is not enough to implement a proper ray-tracing algorithm over parametric surfaces. Additional geometrical parameters or vectors must be derived. The principles of differential geometry [4] have to be applied to calculate the tangent and normal vectors over the parametric nature of the rational surface, figure 2:

- *Tangent vectors*: defined for each parametric direction u and v:

$$\vec{r}_u(u,v) = \frac{\partial \vec{r}(u,v)}{\partial u} = \frac{\partial}{\partial u}\left(\frac{\vec{N}(u,v)}{D(u,v)}\right) = \frac{\frac{\partial \vec{N}(u,v)}{\partial u} D(u,v) - \vec{N}(u,v)\frac{\partial D(u,v)}{\partial u}}{D^2(u,v)} = \frac{\vec{N}^{1,0}(u,v)D(u,v) - \vec{N}(u,v)D^{1,0}(u,v)}{D^2(u,v)} \quad (3)$$

$$\vec{r}_v(u,v) = \frac{\partial \vec{r}(u,v)}{\partial v} = \frac{\partial}{\partial v}\left(\frac{\vec{N}(u,v)}{D(u,v)}\right) = \frac{\frac{\partial \vec{N}(u,v)}{\partial v} D(u,v) - \vec{N}(u,v)\frac{\partial D(u,v)}{\partial v}}{D^2(u,v)} = \frac{\vec{N}^{0,1}(u,v)D(u,v) - \vec{N}(u,v)D^{0,1}(u,v)}{D^2(u,v)} \quad (4)$$

where

$$\vec{N}^{r,s}(u,v) = \frac{\partial^{r+s}\vec{N}(u,v)}{\partial u^r \partial v^s} = \frac{m!n!}{(m-r)!(n-s)!}\sum_{i=0}^{m-r}\sum_{j=0}^{n-s}\Delta^{r,s}(w_{ij}\vec{p}_{ij})B_i^{m-r}(u)B_j^{n-s}(v)$$

$$D^{r,s}(u,v) = \frac{\partial^{r+s}D(u,v)}{\partial u^r \partial v^s} = \frac{m!n!}{(m-r)!(n-s)!}\sum_{i=0}^{m-r}\sum_{j=0}^{n-s}\Delta^{r,s}w_{ij}B_i^{m-r}(u)B_j^{n-s}(v) \quad (5)$$

and

$$\Delta^{r,s}a_{i,j} = \Delta^{r-1,s-1}a_{i+1,j+1} - \Delta^{r-1,s-1}a_{i,j} \qquad \begin{cases} \Delta^{1,0}a_{i,j} = a_{i+1,j} - a_{i,j} \\ \Delta^{0,1}a_{i,j} = a_{i,j+1} - a_{i,j} \\ \Delta^{0,0}a_{i,j} = a_{i,j} \end{cases} \quad (6)$$

- *Normal vector*: defined as the cross product of the tangent vectors:

$$\hat{n}(u,v) = \frac{\vec{r}_u(u,v)\times\vec{r}_v(u,v)}{\left\|\vec{r}_u(u,v)\times\vec{r}_v(u,v)\right\|} \quad (7)$$

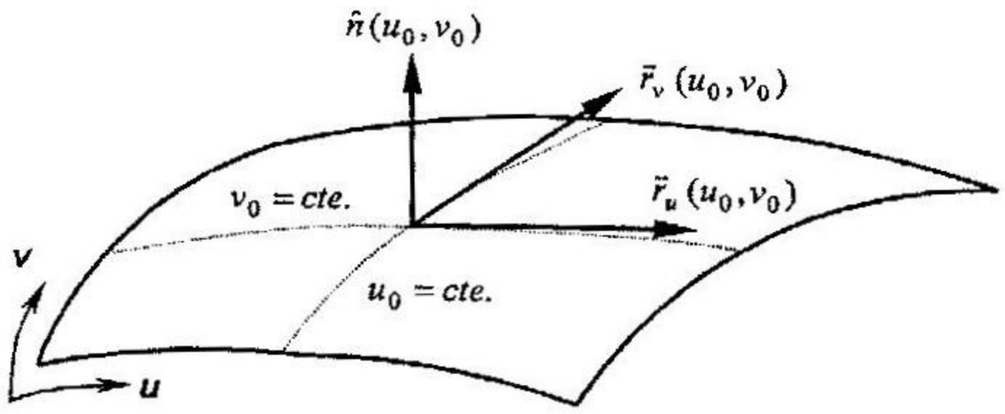

Figure 2: Geometrical vectors of a Bézier surface: tangent and normal vectors.

To sum up, the key point of this geometrical representation resides on its versatility. Figure 3 represents how a Bézier curve, i.e. a one dimensional representation of a Bézier surface, can be easily modified by varying either the position or the weight of one of its control points. The initial curve (white dots) evolves to the new one (black dots) just by changing one of these parameters. If this characteristic is included inside a global optimization scheme, it would be possible to implement a "smart" designing tool able to modify the shape of the mirror surfaces in order to achieve the pursued goal: to maximize the optical path, to minimize the interference effects between adjacent reflection points, to couple the maximum optical power, etc.

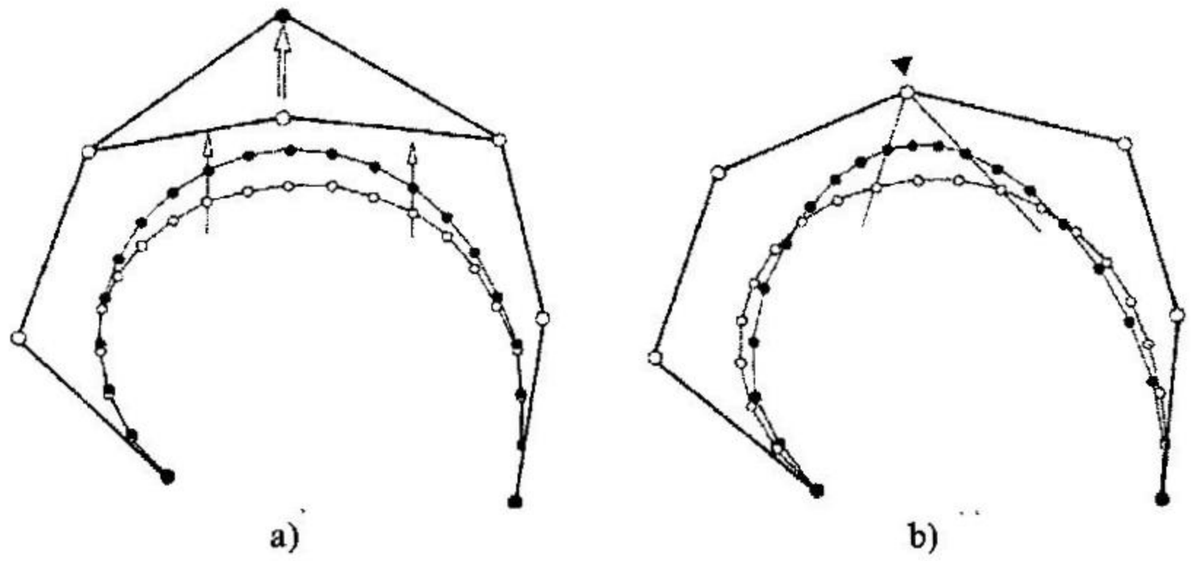

Figure 3: Effects of the modification of the parameters of a Bézier surface: a) modification of the position of a control point, b) modification of the weight of a control point.

For the analysis of the multipass cell, two additional elements have to be taken into account: the ray-tracing mechanism and the modeling adopted for the light source. The first one will be described in Section 3. The light source is represented by its location on the entrance mirror, given in parametric coordinates $\vec{r}_0 = \vec{r}(u_0, v_0)$, the incident direction of the entrance light beam, the number of rays in which the beam is decomposed that will represent the resolution degree of the analysis and by different physical parameters dependent on the illumination:

- A light source is characterized by the beam divergence.
- An optical fiber is represented by its numerical aperture or its radius and refraction index of core and cladding.

3. RAY-TRACING ALGORITHMS

Attending to the ray-tracing mechanisms, two methods have been implemented over the parametric description of the mirrors, i.e. taking advantage of the realistic geometry involved in the problem. Both techniques are defined as non-sequential and allow the analysis of systems with different elements independently of the order of its declaration. Under this operation scheme, light rays are drawn from the optical source and later on modified dynamically when they interact with the elements of the optical system. Likewise, the analysis tool always works with vectorial magnitudes in three

dimensions in order to provide generality to the process and to allow the analysis of arbitrary 3D configurations. The developed ray-tracing techniques are:

- *Fermat's Principle* and *Conjugated Gradient Method (CGM)*: this first ray-tracing algorithm has been generalized for a number of "*N*" bounces inside the cell. Each reflection point "*i*" is denoted by $\vec{r}_i = \vec{r}(u_i, v_i)$. There are two fixed points: $\vec{r}_0 = \vec{r}(u_0, v_0)$ located at the light entrance point and $\vec{r}_{N+1} = \vec{r}(u_{N+1}, v_{N+1})$ that is the point where the light comes out of the cell. Between these defined extreme points, "*N+1*" distances can be formulated reaching an expression for a distance function "*d*" susceptible to be optimized and that is a function of the parametric coordinates (u_i, v_i) of each particular reflection point:

$$d(u_0, v_0, u_1, v_1, \ldots, u_N, v_N, u_{N+1}, v_{N+1}) = \sum_{i=0}^{N} d_i(u_i, v_i, u_{i+1}, v_{i+1}) = \sum_{i=0}^{N} \left\| \vec{r}(u_{i+1}, v_{i+1}) - \vec{r}(u_i, v_i) \right\| = \sum_{i=0}^{N} \left\| \vec{r}_{i+1} - \vec{r}_i \right\| \quad (8)$$

where $\left\| \vec{r}_{i+1} - \vec{r}_i \right\|$ is the Euclidean distance between points $\vec{r}_i$ and $\vec{r}_{i+1}$: $\left\| \vec{r}_{i+1} - \vec{r}_i \right\| = \sqrt{(\vec{r}_{i+1} - \vec{r}_i) \cdot (\vec{r}_{i+1} - \vec{r}_i)}$. To optimize this distance function, and taking into account that the surfaces are typically concave shaped, a maximum in this function should be found by zeroing the gradient of this distance function respect to the parametric coordinates of the reflection points $(u_1, v_1, u_2, v_2, \ldots, u_{N-1}, v_{N-1}, u_N, v_N)$. The Conjugated Gradient Method [6] with the Polak-Ribiere correction has been implemented for this process and the gradient of the distance function "*d*" has been derived analytically for a generic number of reflections "*N*". The solution offered by the numerical optimization algorithm is afterwards validated in terms of accomplishment of the Snell's Law at each bounce.

- *Shooting and Bouncing (S&B)* [7]: the process consists in launching rays, at each reflection point, in the direction that accomplish the Snell's Law. Afterwards, the next reflection point is calculated by formulating an intersection problem between a Bézier surface and the reflected ray from the previous bounce. This intersection problem is solved by applying a new reformulated version of the Conjugated Gradient algorithm. The process finishes when a valid solution is found for the number of bounces specified by the user.

4. RESULTS

The developed techniques (cell representation, light source modelling and ray-tracing techniques) have been validated comparing the achieved configurations and results with analytical models, commercial optical design systems, structures found in literature, etc. If the new numerical tool is able to reproduce these results, one can infer its validity in the analysis of novel an arbitrary multipass cells. The results are given in terms of achieved optical path length and composed reflection patterns that represent the position of reflection points in both mirrors of the cell.

- *Multipass cell with flat mirrors*: this first test has been selected due to its easy validation through analytical calculation of the reflection points. When the ray-tracing algorithms are compared, both of them behave correctly. Figure 4 represents the dimensions and the resulting ray-tracing.

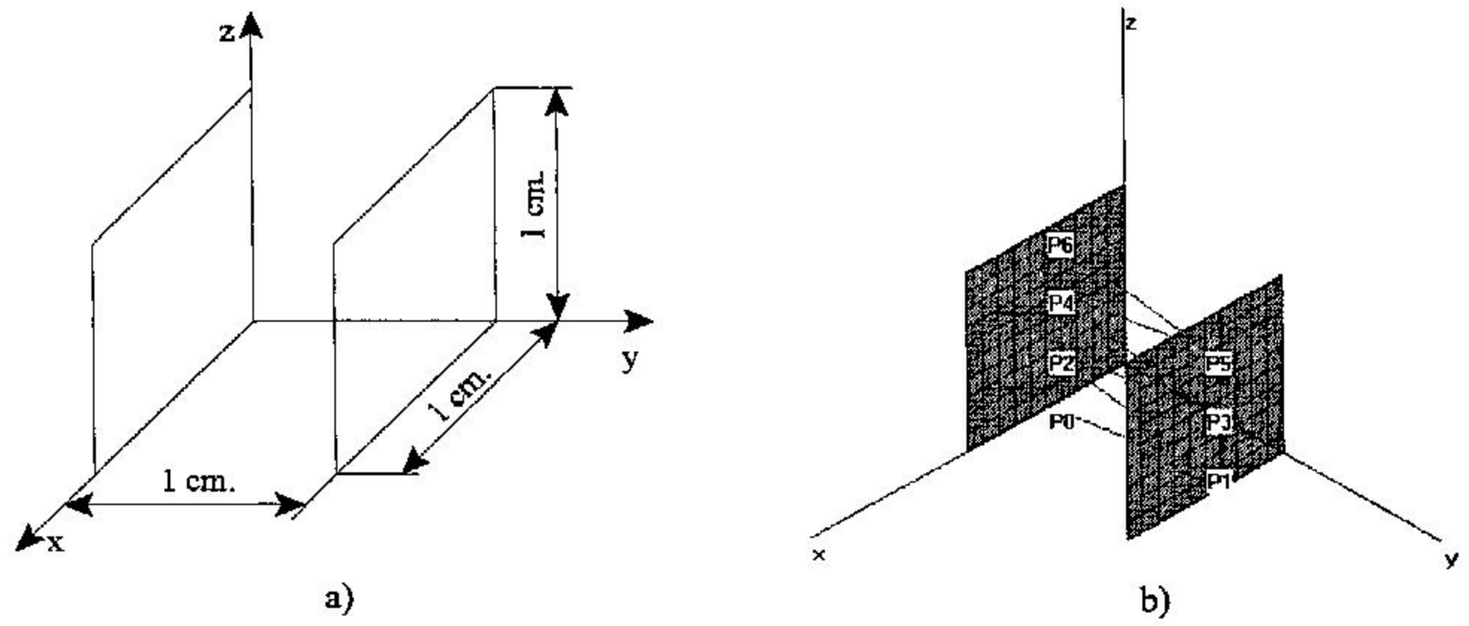

Figure 4: Multipass cell with flat mirrors: a) cell definition, b) ray-tracing.

- *Multipass cell with convex mirrors*: this case introduces the analysis of non-flat surfaces. Figure 5 illustrates the dimensions and separation of the spherical convex surfaces employed to model the mirrors. Each mirror is represented with one Bézier surface.

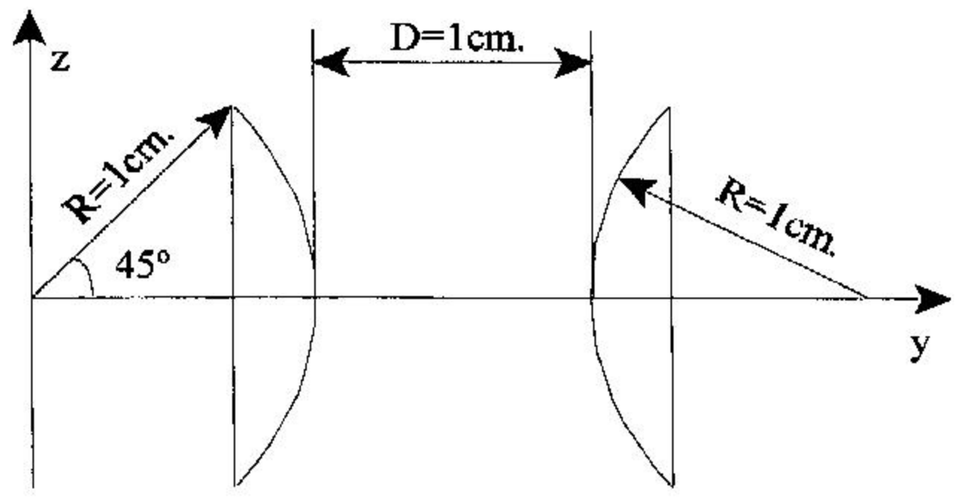

Figure 5: Multipass cell definition with convex spherical mirrors.

Results in terms of composed reflection pattern and ray-tracing are provided in figure 6. This kind of cell has been created to validate and compare the implemented ray-tracing techniques from a functionality point of view. It has no direct application in the gas detection field because as the number of reflections is increased, in order to maximize the path length, the beam tends to concentrate around the centers of the surfaces magnifying the interference effects among beams. From the ray-tracing side, the result has been confronted with commercial optical design software called ZEMAX® from *Focus Software* [8]. Both CGM and S&B presents good results when compared with ZEMAX® that represent the mirrors as canonical truncated spheres. As the number of reflections increased, the CGM suffers from problems in convergence because the distance function becomes nearly flat without a pronounced maximum.

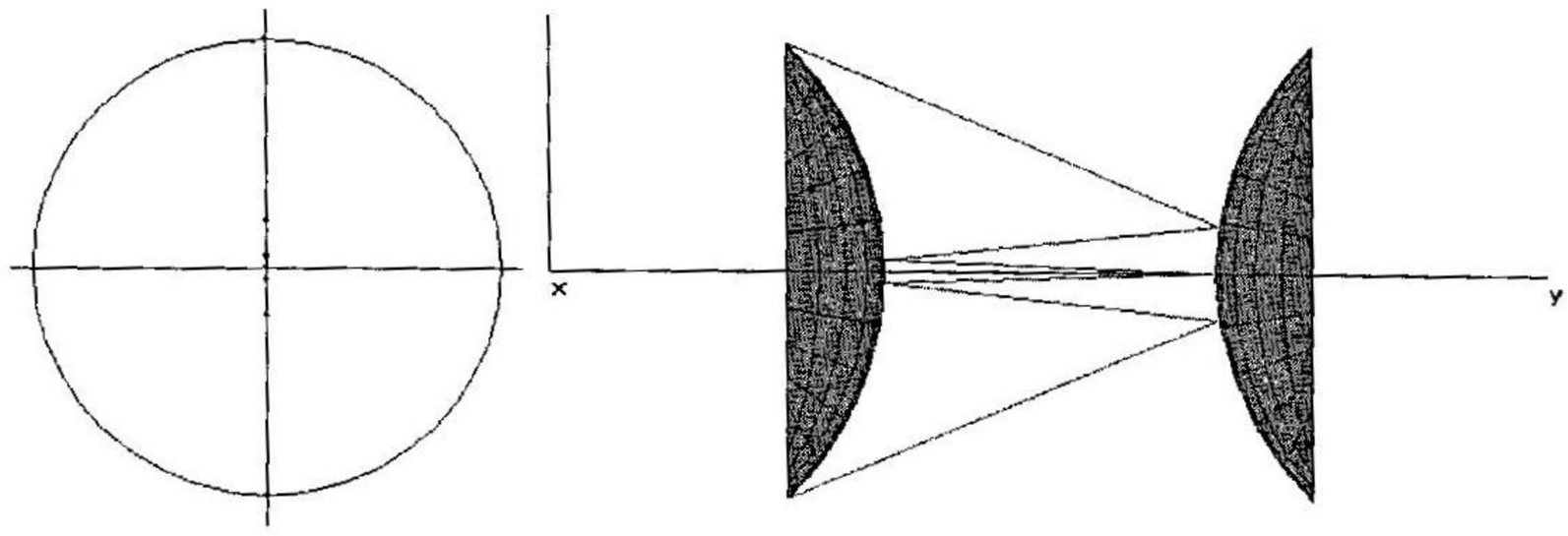

Figure 6: Composed reflection pattern and ray-tracing for the cell conformed by convex spherical surfaces. Parameters of the analysis: 5 reflections, $d = 1\ cm$, mirror radius $r = 1\ cm$, $(x_0, y_0, z_0) = (0, 0.707, -0.707)$.

- *Multipass cell with concave mirrors*: several references appeared in literature have been reproduced and analyzed with the developed tool. Most of them are based in mirrors that follow canonical geometries such as spherical [9] or parabolic [10] that in the references are analyzed following an analytical strategy. Figure 7 represents the multipass cell described in [10].

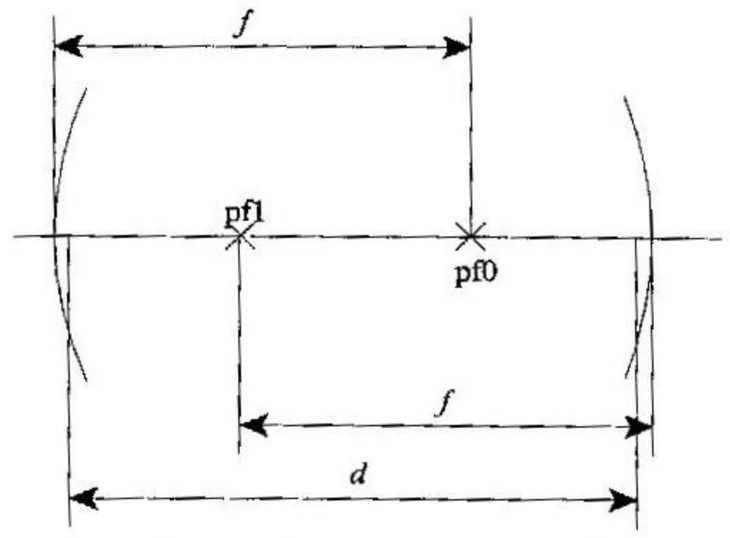

Figure 7: Multipass cell definition with parabolic mirrors.

In this configuration, with entrance point (x_0, y_0, z_0) and direction tangent of the ray $(x_0', 0, z_0')$, the reflection points after N passes are located over the mirrors in the plane $y=y_0$ [10] at the points:

$$x_n = x_0 \cos(n\theta) + \sqrt{\frac{d}{4f-d}}(x_0 + 2fx_0')\sin(n\theta)$$
$$z_n = z_0 \cos(n\theta) + \sqrt{\frac{d}{4f-d}}(z_0 + 2fz_0')\sin(n\theta) \qquad (9)$$

where $\cos\theta = 1 - \left(\frac{d}{2f}\right)$. When the location coordinates of the entrance point are $x_0 = \sqrt{\frac{d}{4f-d}}(z_0 + 2fz_0')$ and $z_0 = x_0 + 2fx_0' = 0$, the reflection points on both mirrors conform a circular pattern with radius $r_1 = x_0$ and coordinates $x_n = x_0 \cos n\theta$ and $z_n = x_0 \sin n\theta$. As for the case of convex surfaces, the only ray-tracing method valid for this analysis is the S&B. The result of the developed tool is depicted in figure 8, where the composed reflection pattern in both mirrors is represented. As expected, in this case, this reflection pattern is perfectly circular.

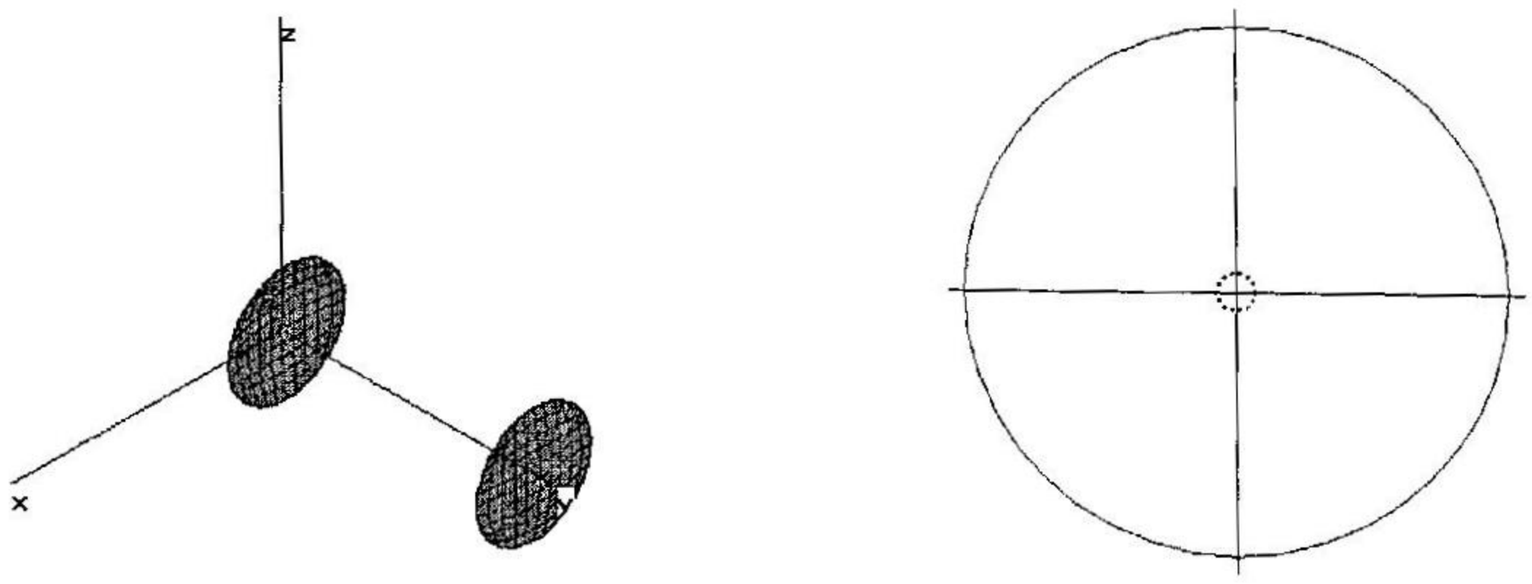

Figure 8: Configuration and composed reflection pattern for a multipass cell with parabolic mirrors. Parameters of the analysis: 13 reflections, $f = 10\ cm$, $d = 15.54\ cm$, mirror radius $r = 3.53\ cm$, $(x_0, y_0, z_0) = (0.25,0,0)$.

5. CONCLUSIONS

This contribution presents a new tool for the analysis and posterior design of multipass gas cells. The tool takes the advantage of a very flexible and versatile representation of the mirrors in terms of parametric surfaces known as NURBS. As NURBS surfaces are highly widespread in the field of solid modeling, the manufacturing process will find no problem in replicating the final designed cell. Based on this geometrical representation, two different ray-tracing algorithms have been implemented, one based on the optimization of a distance function and another based on the idea of shooting and bouncing of rays. Taking into account that, in order to reach optical confinement into the cell, the mirror surfaces are mainly concave shaped, the algorithm of shooting and bouncing attains a better behavior when compared with the optimization of the distance function because the last one finds difficulties during the convergence process. Results have been validated with analytical and published works found in literature in order to test if the obtained reflection patterns are correct. Due to the flexibility of the surface representation, works are in progress in order to evaluate the sensibility to manufacturing tolerances and alignment processes.

ACKNOWLEDGEMENTS

Authors thank the Spanish Government under the Ministry of Science and Technology for its support through the EOAMOP (TIC'2002-01259) R&D project.

REFERENCES

1. J.U.White, "Long optical paths of large aperture", *J.O.S.A.*, Vol.32, pp.285-288, 1942.
2. D.R.Herriott, J.U.White, "Long optical paths of large aperture", *J.O.S.A.*, Vol.32, pp.285-288, 1942.
3. J.B.McManus, P.L.Kebabian, M.S.Zahniser, "Astigmatic mirror multipass absorption cells for long-path-length spectroscopy", *Applied Optics*, Vol. 34, pp.3336-3348, 1995.
4. Gerald Farin, '*Curves and surfaces for CAGD*', Academic Press, 3rd Ed, 1993.
5. C. de Boor, "On calculating with B-Splines", *J. Approx. Theory*, Vol. 6, No. 1, pp.50-62, 1972.
6. W. H. Press, B. P. Flannery, S. A. Teukolsky and W. T. Vetterling, '*Numerical Recipes*', Cambridge University Press, 1987.
7. H.Ling, R-C.Chou, S-W Lee, "Shooting and bouncing rays: calculating the RCS of an arbitrarily shaped cavity", *IEEE Transactions on Antennas and Propagation*, Vol. 37, No. 2, pp.194-205, 1989.
8. ZEMAX®, *Focus Software Inc.* (www.focus-software.com).
9. W.R.Trutna, R.L.Byer, "Multiple-pass Raman gain cell", *Applied Optics*, Vol.19, No.2, pp.301-312, 15 January 1980.
10. J. Altmann, R. Baumgart, C. Weitkamp, "Two-mirror multipass absorption cell," *Applied Optics*, Vol.20, No.6, pp.995-999, March 1981.